Case Studies in Construction Materials 23 (2025) e04984

Contents lists available at ScienceDirect

Case Studies in Construction Materials

journal homepage: www.elsevier.com/locate/cscm

Case study

Hybrid fiber-reinforced geopolymer composites with enhanced impact resistance for marine structures

Yun Xu [a,1], Yichen Zhou [b,*,1], Ke Zhuang [a,*], Haoliang Wu [c,d], Qian Zhang [a], Kai Zhou [a], Boyin Ding [b], Xiaohuan Meng [a], Ziqun Wang [a], Zhenqiu Hu [b], Jingming Cai [b]

[a] *State Key Laboratory of Low-carbon Smart Coal-fired Power Generation and Ultra-clean Emission, China Energy Science and Technology Research Institute Co.,Ltd., Nanjing 210023, China*
[b] *Key Laboratory of Concrete and Prestressed Concrete Structures of Ministry of Education, Southeast University, Nanjing 211189, China*
[c] *Dongguan Institute, Sun Yat-sen University, Dongguan 523808, China*
[d] *School of Civil Engineering, Sun Yat-sen University & Southern Marine Science and Engineering Guangdong Laboratory (Zhuhai), Zhuhai 519082, China*

ARTICLE INFO

Keywords:
Engineered geopolymer composites (EGC)
Low-velocity impact
PVA fiber
PE fiber
Marine construction materials

ABSTRACT

To address the growing demands for corrosion-resistant marine infrastructure in chloride-rich environments, the mechanical properties and damage mechanisms of engineered geopolymer composites (EGC) reinforced with polyvinyl alcohol (PVA) fiber blends and polyethylene (PE) fiber blends under low-velocity impact were investigated in this study. By preparing EGC specimens reinforced with PVA/PE fiber blends with different volume doping (0–2 %), uniaxial tensile, compressive and low-velocity impact experiments were carried out to analyze the effects of fiber blending ratios on the material properties. The results showed that the PVA fibers enhanced the interfacial bonding through hydroxyl bonding, which significantly increased the tensile and compressive strengths of the materials, while the PE fibers exhibited excellent crack control and energy dissipation ability under impact loading due to their high specific surface area and hydrophobicity. During pseudo-static loading, the crack control ability of PVA fiber specimens was better than that of PE fiber specimens; however, PE fiber specimens were able to form a more homogeneous microcrack network under low-velocity impact. The PE/PVA fiber hybrid system (EGC-0.5–1.5) has comprehensive advantages in tensile ductility (7.86 %) and tensile strength (3.85 MPa), making it suitable for high impact demand scenarios. The pure PVA fiber hybrid system (EGC-2–0) can control the tensile crack width to around 39 μ m, while reducing the cost by 14–39 % compared to the PE fiber system. It is suitable for engineering scenarios that require strict crack control and economic considerations.

1. Introduction

In recent years, researchers have developed engineered cementitious composites (ECC) by incorporating different types of fiber

* Corresponding authors.
E-mail addresses: 220231330@seu.edu.cn (Y. Zhou), 12083096@ceic.com (K. Zhuang).
[1] Co-first author.

https://doi.org/10.1016/j.cscm.2025.e04984
Received 8 May 2025; Received in revised form 22 June 2025; Accepted 26 June 2025
Available online 26 June 2025

reinforcement materials into cementitious concrete [1]. This material shows excellent ductility and cracking resistance by achieving multiple cracking and pseudo strain hardening behavior under tensile and flexural loading [2,3]. Based on ECC, researchers have further explored more environmentally friendly alternatives by preparing engineered geopolymer composites (EGC) using mineral materials rich in aluminum-silica components (e.g., fly ash, ground granulated blast furnace slag, metakaolin, and red mud, etc. [4–6]) instead of conventional cement. This innovation not only significantly reduces carbon emissions, also performs outstandingly in terms of ductility, durability, and impact resistance [4,7–10], and provides a new direction for the development of sustainable building materials.

The properties of fibers, as a key material for enhancing the ductility of concrete, have been the focus of researchers' attention [11, 12]. Due to the differences in raw materials, physical and chemical properties, and production processes, the performance and cost of different fibers vary greatly [13]. Polyvinyl alcohol (PVA) and polyethylene (PE) fibers are two commonly used fibers. The PVA fibers have a large number of hydroxyl groups (-OH) in their molecular chains [14], enabling the formation of hydrogen bonds with water molecules, and this hydrophilicity leads to a very tight bond with the geopolymer matrix as well as to their low tensile strength, which makes them susceptible to fracture. On the contrary, PE fibers have hydrophobicity as well as excellent mechanical properties [15] and can achieve steady-state multi-crack extension through controlled interfacial debonding, but at 2–8 times the cost of PVA fibers [16]. Additionally, the embodied carbon and embodied energy generated during the production of PVA fibers is 20 % lower than that of PE fibers [17], and PVA fibers are biodegradable [18], which provides a significant competitive advantage in the field of green building and low-carbon engineering.

As a high-performance construction material, engineered geopolymer composites show a broad application prospect in the construction of infrastructure [19] such as protective works, bridges, tunnels, etc., by virtue of their excellent compressive strength and tensile ductility [20]. However, in the actual engineering environment, these infrastructures are often subjected to low-velocity impacts (<10 m/s), such as vehicle collisions [21], rockfall impacts [22] and ship impact [23], which may lead to structural damage. Therefore, the mechanical response and damage mechanism of EGC under low-velocity impacts have become a research hotspot and have received extensive attention [4,24–26]. In addition, PVA fibers and PE fibers have significant complementary properties in performance, and mixing PVA fibers and PE fibers at the same time in concrete materials can give full advantage to the two kinds of fibers and optimize the comprehensive performance of the materials [27]. Soe et al. investigated the impact resistance of hybrid fiber engineered cementitious composite boards and found that hybrid fiber ECC is superior in terms of impact resistance [28]. Currently, many studies have been conducted to explore the mechanical properties, self-healing characteristics, and bonding behavior of PVA/PE hybrid fiber-reinforced engineered geopolymer composites with concrete matrix [27,29,30], but the study of their dynamics is still relatively limited.

Thus, this study focuses on the mechanical response and damage mechanism of engineered geopolymer composites (EGC) reinforced with PVA/PE hybrid fibers under low-velocity impact. The fly ash-based one-part engineered geopolymer composites were prepared by using PVA fibers and PE fibers with different volume doping (0–2 %). The study first analyzed the differences in uniaxial tensile and compressive properties of EGC with different fiber ratios. Subsequently, the energy dissipation and damage mechanisms of the specimens under different impact energies were further explored based on the data recorded by the drop hammer testing machine, the damage patterns and micro-morphology of the samples. Finally, the advantages and disadvantages of PVA fibers and PE fibers were compared through statistical analysis of the data, and the overall performance of EGC was comprehensively evaluated in terms of four aspects, including tensile ductility, compressive performance, impact energy absorption capacity and cost.

2. Experimental program

2.1. Raw materials and mixing proportions

The morphology of each raw material is shown in Fig. 1. The precursors used in this study were fly ash (FA), ground granulated blast furnace slag (GGBS) and calcium carbide slag (CCS), with fly ash grade F and GGBS grade S95, and calcium carbide slag was used

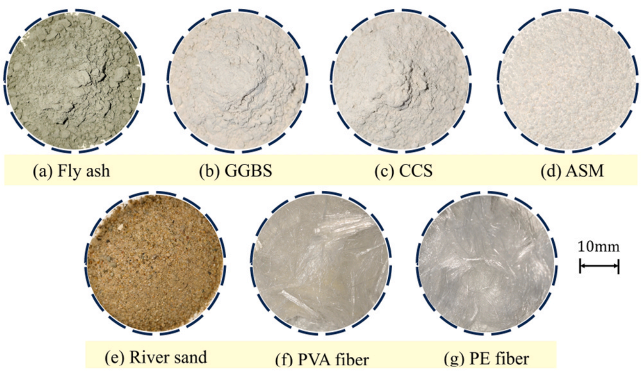

Fig. 1. Raw materials.

as a precursor in order to provide an alkaline environment to activate the FA, and to promote the production of hydrated calcium silicate or hydrated calcium silica-aluminate [31], in order to increase the pre-existing strength of the geopolymer. The average particle sizes of FA, GGBS and CCS were 18.2μm, 17.4μm and 28.9μm, respectively, and their composition is shown in Table 1, the use of smaller particle sizes increases the strength of the geopolymer [32]. The use of anhydrous sodium metasilicate ($SiO_2/Na_2O = 0.91$, by mass) as a solid alkali exciter in place of liquid waterglass can improve the safety of the production process [4,33]. The fine aggregate was washed natural river sand with a fineness modulus of 2.7 and a mud content of 0.7 %. The fibers used for the preparation of EGC were PVA fibers and PE fibers, respectively, and the specific physical properties are shown in Table 2. The water reduction rate of the high-range water-reducing admixture (HRWR) used was 30 %, adding HRWR reduces water consumption and increases the workability of freshly mixed slurries [34].

The mixing proportions of EGC are shown in Table 3. Because 2 % by volume fiber dosing is the optimal dosing level suggested by a large number of researchers [35], keeping the 2 % volume doping of fibers unchanged and changing only the ratio of the two types of fibers to investigate the effects of PVA fibers and PE fibers on the uniaxial tensile properties, compressive properties and impact resistance of EGC.

2.2. Specimen preparation and test methods

Fig. 2 summarizes the general preparation of the specimens. Firstly, the precursor was mixed with river sand for 1 min, then water and HRWR were added and stirred for 2 min. After mixing the slurry well, PVA fibers and PE fibers were added slowly, and they should be added alternately and stirred thoroughly to ensure that the two types of fibers were well dispersed. After reaching the optimum fiber dispersion, the freshly blended pastes were loaded into the respective molds at 20 ± 3°C [36] and 70 ± 5 % humidity [37], and the experiments were carried out after 7 and 28 days of curing, respectively. The uniaxial tensile test, compressive performance test each group using three specimens for the experiment, the data results take the average value, the impact resistance test using a specimen for the experiment.

The experimental apparatus as well as the dimensions of the specimens are shown in Fig. 3. Fig. 3**(a)** shows the uniaxial tensile experiment, which was conducted using a dog bone shaped specimen according to the recommendation of the JSCE [38], with a tensile rate of 0.5 mm/min. The experimental apparatus was a universal testing machine with an LVDT device (Type WDW-500E, DROIDE Co., Ltd, China). The accuracy of the recorded displacement data was 0.1 mm, and the compression test was also conducted with this instrument, and the specimen size of the compression test was a cube of 70.7 × 70.7 × 70.7 mm.

Fig. 3**(b)** shows the impact experiments, which were carried out using an automatic drooping hammer test machine (Type CEAST-9350, Instron Co., Ltd, United States). The weight of the hammer head was 3.41 kg, and the drop height was controlled so that the hammer has kinetic energies of 9 J, 12 J and 15 J respectively when contacting the impact specimen after free fall. Impact displacement (δ_t), impact force (F_t), impact velocity (v_t), are able to be recorded by the sensors inside the hammer head. Impact energy (E_t) is the energy absorbed by the test piece and is calculated as follows [39]:

$$v_t = v_0 + gt - \int_0^t \frac{F(\tau)}{m} d\tau \tag{1}$$

$$\delta_t = \delta_0 + v_0 t + \frac{gt^2}{2} - \int_0^t \int_0^t \frac{F(\tau)}{m} d^2\tau \tag{2}$$

$$E_t = \frac{m[v_0^2 - v_t^2(t)]}{2} + mg\delta(t) \tag{3}$$

$m$is the weight of the hammer head, $g$is the acceleration due to gravity.

Where impact energy (E_t) includes the energy dissipated by the specimen (E_d) and the kinetic energy of the specimen and hammer head after impact (E_K), and (E_K) is much smaller when the specimen remains integrity, less than 0.1 % of (E_d). Therefore, (E_K) is ignored in the calculation and the energy dissipation coefficient is calculated from the following formula:

$$E_t = E_d + E_K \approx E_d \tag{4}$$

$$\varphi = \frac{E_d}{E_s} = \frac{E_t}{E_s} \tag{5}$$

E_s is the impact of energy of the hammer when it contacts the specimen.

Table 1
Chemical composition of precursors (wt%).

Compositions	CaO	SiO_2	Al_2O_3	MgO	SO_3	Fe_2O3	Na_2O	TiO_2	K_2O
Fly ash	9.86	46.61	25.98	2.79	1.21	6.89	1.93	1.83	2.55
GGBS	36.71	29.80	17.46	9.02	2.44	0.91	0.62	0.32	0.58
CCS	91.3	3.24	2.08	0.41	1.01	0.51	0.21	0.15	0.34

Table 2
Physical properties of fibers.

Fiber type	Density (g/cm^{-3})	Length (mm)	Diameter (μm)	Elastic Modulus (GPa)	Tensile Strength (MPa)
PVA	1.29	12	51	36	1580
PE	0.98	12	18	105	3210

Table 3
Mixing proportions of EGC.

Type	FA	GGBS	CCS	Alkaline activator	Water	River sand	PVA fiber (vol%)	PE fiber (vol%)	HRWR
EGC−2–0	0.55	0.33	0.06	0.06	0.36	0.5	0.02	0	0.01
EGC−1.5–0.5	0.55	0.33	0.06	0.06	0.36	0.5	0.15	0.05	0.01
EGC−1–1	0.55	0.33	0.06	0.06	0.36	0.5	0.01	0.01	0.01
EGC−0.5–1.5	0.55	0.33	0.06	0.06	0.36	0.5	0.05	0.15	0.01
EGC−0–2	0.55	0.33	0.06	0.06	0.36	0.5	0	0.02	0.01

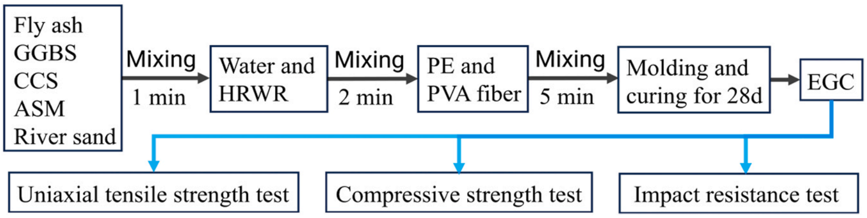

Fig. 2. Specimen preparation process.

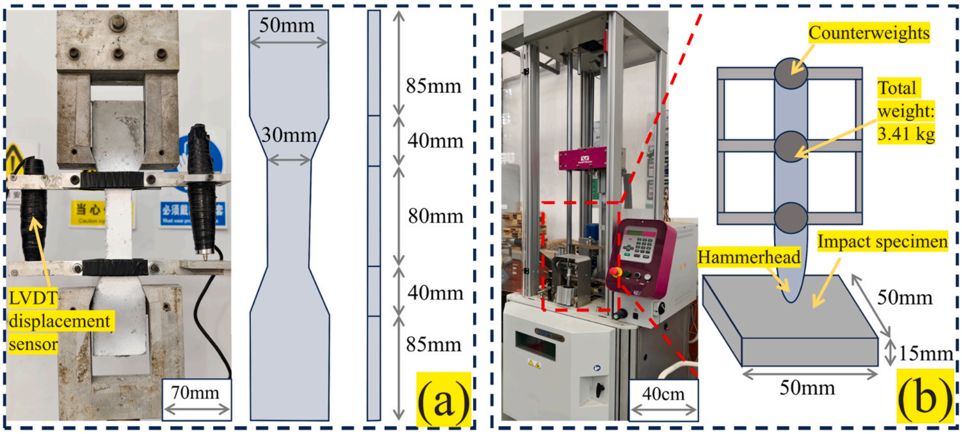

Fig. 3. Experimental apparatus.

3. Uniaxial tensile properties and compressive properties of EGC

The results of the uniaxial tensile experiments of EGC are shown in Fig. 4**(a)** and Table 4, where the initial crack strength indicates the tensile stress to which the specimen is subjected at the appearance of the first crack, the ultimate tensile strength indicates the maximum tensile stress to which the specimen is subjected, and the ultimate tensile strain indicates the strain in the strain-softening stage when the magnitude of the tensile stress to which the specimen is subjected is 80 % of the ultimate tensile strength. The average crack width and the average number of cracks were obtained by averaging the three sets of data, measurement range is within 80 mm of the center of the tensile specimen. It is noticed that the initial crack strength and ultimate tensile strength of the specimens maintain a decreasing trend as the PE fiber doping increases from 0 % to 2 %. Among them, the initial crack strength and ultimate tensile strength decreased the most when the PVA fiber doping was reduced from 1 % to 0.5 %, up to 17.3 % and 14.1 %, correspondingly. Furthermore, the ultimate tensile strain maintains an increasing trend, and the ultimate tensile strain of 2 % doped PE fiber is 2.36 times higher than that of 2 % doped PVA fiber. It can be concluded that increasing the PVA fiber doping is beneficial to increase the

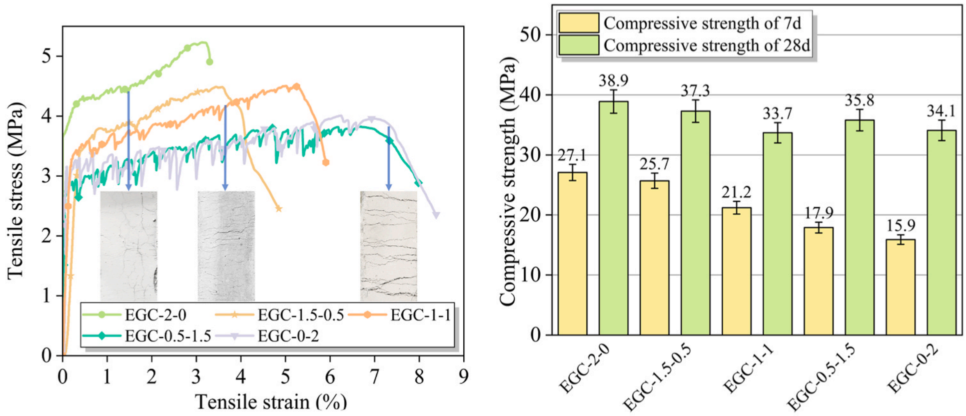

(a) Uniaxial tensile test

(b) Compression test

Fig. 4. Uniaxial tensile test and compression test results.

Table 4
Uniaxial tensile test results.

	Initial crack strength (MPa)	Ultimate tensile strength (MPa)	Ultimate tensile strain (%)	Average number of cracks	Average crack width (μm)
EGC−2–0	3.64	5.22	3.30	73	39
EGC−1.5–0.5	3.38	4.49	4.11	69	51
EGC−1–1	3.28	4.48	5.81	54	93
EGC−0.5–1.5	2.71	3.85	7.86	39	166
EGC−0–2	2.63	4.00	7.78	31	208

tensile strength of EGC under the pseudo-static load, while increasing the PE fiber doping is beneficial to increase the tensile ductility of EGC.

It is worth noting that excessive crack width reduces the durability of EGC [40].The average crack widths of EGC-0.5–1.5 and EGC-0–2 reached 166μm and 208μm, respectively, which were 1.78 and 2.23 times higher than that of EGC-1–1, while the tensile ductility was only increased by 35.3 % and 33.9 %, respectively, compared with that of EGC-1–1. The reason for this phenomenon may be the weak bonding between PE fibers and geopolymer matrix [41], so the doping of PE fibers should not be more than 1 % when EGC is needed to have strong crack control ability. Additionally, based on experimental data from other researchers, the average crack width range for PVA-ECC is 70–130 μm [42], while the average crack width range for PE-ECC is 80–200 μm [43]. This indicates that PVA-ECC has stronger crack control capabilities, while PE-ECC and PE-ECC have similar performance.

The results of 7d and 28d compressive experiments of EGC are shown in Fig. 4**(b)**. A high PVA doping ratio can be found to have higher compressive strength at the early stage of EGC maintenance, and the compressive strength is inversely proportional to the PE fiber doping. The 7d strength of EGC-2–0 is 1.70 times that of EGC-0–2, but the 28d strength is only 1.14 times that of EGC-0–2. In the early stage of material maintenance, the friction strength between the PE fiber and matrix interface is at a low level [44]. It is difficult to form an effective stress transfer mechanism at the interface between the fiber and matrix at this stage [45], resulting in the PE fiber not being able to effectively inhibit the expansion of microcracks, but instead introducing more defects within the interface transition zone, resulting in a decrease in the strength of EGC. At 28 d, the strength difference between the mixing proportions of EGC was small, a phenomenon that indicates that the influence effect of fiber type parameters on the late strength development of the material is gradually weakening. At this mature stage, the degree of microstructural densification of the geopolymer matrix and the mechanical properties of its hydration products become the decisive factors dominating the macroscopic compressive strength properties of EGC [46].

4. Impact resistance

4.1. Impact energy of 9J

When the impact energy is 9J, the force-displacement curve (a), force-time curve (b) and energy dissipation coefficient (c) of EGC after impact are shown in Fig. 5. The larger impact force of EGC-2–0 compared to the other groups can be found, which indicates that it has greater impact stiffness. Another remarkable feature of the impact force-displacement curves of EGC-2–0 is that there is no plateau segment, and the impact force decreases rapidly after reaching the peak value. The reason for the plateau segment is that the fiber bridge effect makes the fibers bear parts of the impact force [47], and the force-holding fibers are pulled out from the geopolymer matrix, which leads to the creation of new cracks. The new cracks keep the total friction of the fibers during pullout essentially constant, while a small portion of the fibers break, so the impact force stays in a small range of fluctuation [4]. At the same impact displacement, the impacts of EGC-2–0 and EGC-1.5–0.5 took longer, probably due to the good interfacial bonding between the PVA fibers and the geopolymer matrix and greater elongation at break [48], which allowed the specimens to dissipate energy mainly through the fracture of the PVA fibers themselves instead of friction, which could explain the higher energy dissipation coefficient for a PVA fiber doping of 2 % and the absence of a plateau segment in the impact curve.

The damage pattern at an impact energy of 9J is shown in Fig. 6, where the integrity of the impact specimen can be maintained at the 9J impact energy, and it can be found that the number of cracks on the tensile surface of the impact specimen increases, and the crack width decreases with the increase of PE fiber doping. It is worth noting that this is contrary to the results of uniaxial tensile experiments, where PVA fibers have better crack control in the pseudo-static test at a strain rate of 0.0001 s^{-1}, while PE fibers have better crack control at low impact speeds at a strain rate of 1–10s-1, the strain rate is approximated as the strain during loading divided by the loading time.

4.2. Impact energy of 12J

The impact force, impact displacement and duration of the impact specimen increased when the impact energy was 12J, as shown in Fig. 7. At this point, the impact displacement and duration of EGC-2–0 increased significantly, but the strain rate remained in the range of 1–10 s^{-1}, and the impact displacement reached 11.4 mm, which was 76 % of the specimen thickness, at this time, the specimen was close to being pierced, but the specimen still maintained its integrity before the impact energy was completely dissipated, and the energy dissipation coefficient reached 99.1 %, which indicated that the PVA-EGC had a good energy dissipation ability before being pierced. Additionally, the energy dissipation coefficient of the EGC specimen with PE fibers was slightly lower than that of EGC-2–0, but the difference was only within 1.3 %.

The damage pattern at an impact energy of 12 J is shown in Fig. 8. Compared with the 9 J impact energy, the specimens containing PE fibers showed an increase in the number of cracks and the average crack width, and the cracks were radially or reticulately distributed along the force points of the drop hammer impact, with a wider main crack connected to several to dozens of fine cracks, which resulted in a more even distribution of the impact damage in the specimens [49]. On the other hand, EGC-2–0 still maintains a smaller number of cracks and a larger crack width, which is not conducive to the durability of EGC in service condition [50].

4.3. Impact energy of 15J

When the impact energy is 15J, the results of the impact experiments of EGC are shown in Fig. 9, and the impact force and impact displacement of the impact specimens further increase. It is worth noting that at this time, the force-displacement curves of EGC-1.5–0.5 exhibit similar characteristics to those of EGC-2–0 at 9J and 12J impact energy, i.e., the impact force reaches the peak and then decreases rapidly, and the reason for this phenomenon may be that the impact force is too large, which makes the specimen more inclined to the dilation of the old cracks than to the generation of the new cracks in the impact process. In addition, it can be found that the energy dissipation coefficient of EGC-2–0 is only 58.5 %, which is reasonable. First, as shown in Fig. 10, it was observed that EGC-2–0 broke into several small pieces after being impacted by the drop hammer, and a large portion of the energy in the form of kinetic energy was absorbed by the fragments of the impacted specimen [51]. Secondly, the action time of the impact was only 2.2 ms, and when the specimen was destroyed, the hammer head still had a certain velocity in the free-fall direction, and this part of the kinetic energy was not absorbed by the impacted specimen. Therefore, it can be concluded that EGC doped with PE fibers exhibit greater strain energy density and superior impact energy dissipation compared to conventional EGC reinforced with PVA fibers [45].

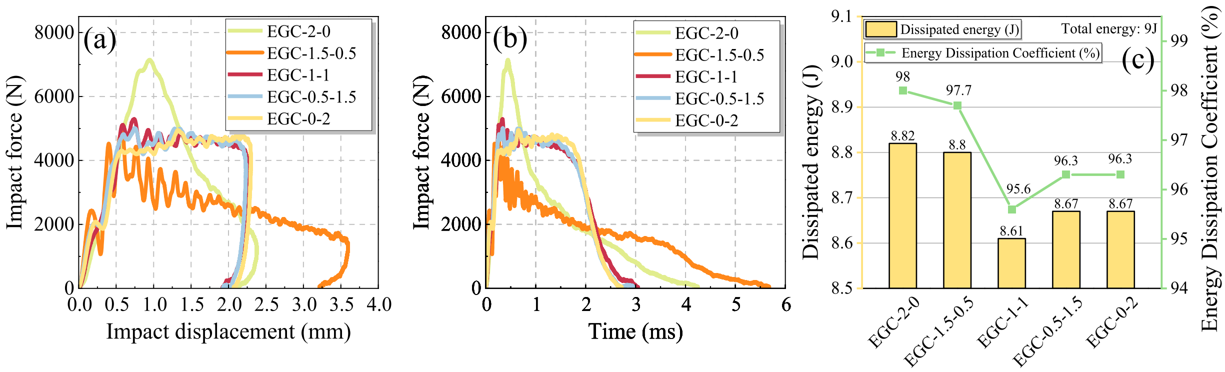

Fig. 5. Results of impact experiment (9 J).

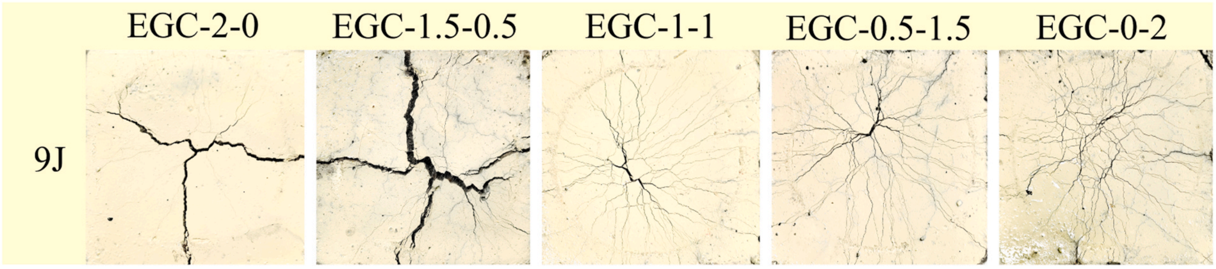

Fig. 6. Damage pattern of impact specimen (9 J).

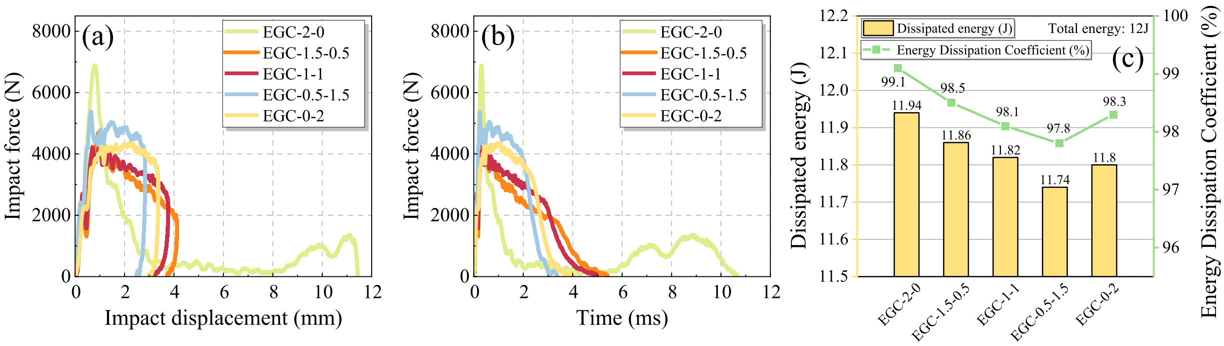

Fig. 7. Results of impact experiment (12 J).

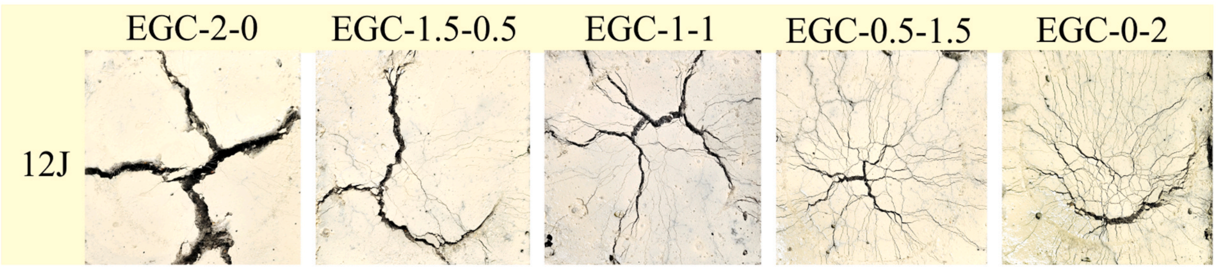

Fig. 8. Damage pattern of impact specimen (12J).

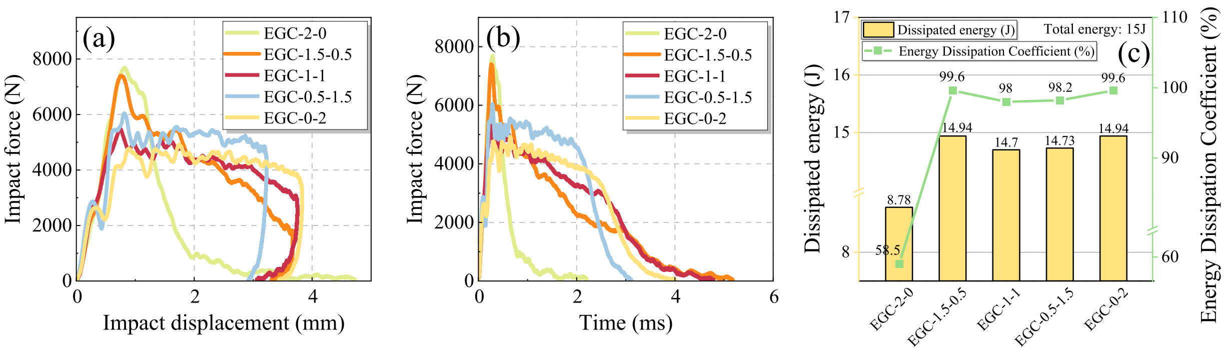

Fig. 9. Results of impact experiments (15 J).

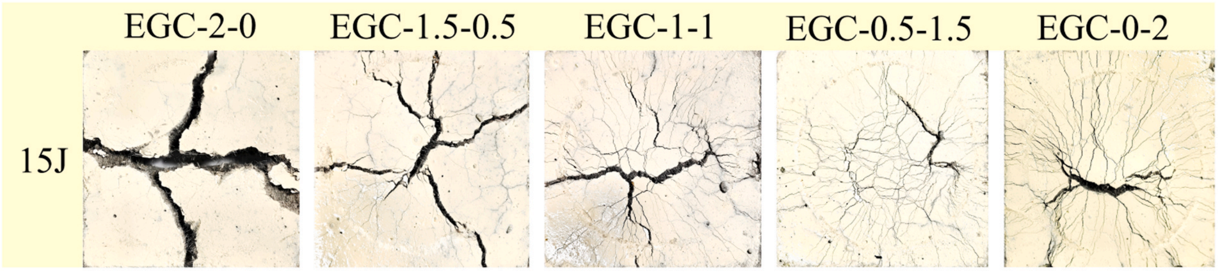

Fig. 10. Damage pattern of impact specimen (15 J).

4.4. Microscopic morphology of impact specimens

The micro-morphological analysis of the specimens under 15J impact energy (Fig. 11) reveals that the surface of the PVA fibers in specimen EGC-2–0 exhibit localized friction traces and transverse fractures distributed along the radial direction of the fibers, which indicates that the fiber system achieves energy dissipation through the dual mechanism of frictional slip at the fiber-substrate interface and tensile fracture of the fibers. It is worth noting that the two types of fibers in the EGC-1–1 specimen show significantly different failure modes: compared with PVA fibers, PE fibers show a significant increase in surface roughness and form continuously distributed friction tracks, and a large number of exfoliated particles of the geopolymer matrix are visible on their surfaces (with particle sizes concentrating on 2–5μm), which is attributed to the continuous friction of PE fibers to exfoliate particles of the matrix, which is inferred to be the main factor of energy dissipation in the system. This phenomenon is attributed to the stripping of matrix particles by PE fibers through continuous friction action, and it can be inferred that the friction dissipation accounts for a high proportion of their total energy absorption [52]. In particular, the PE fibers in the EGC-0–2 specimen showed a denser distribution (fiber spacing <50μm). Since the diameter of PE fibers (18μm) is only 35 % of that of PVA fibers (51μm), their higher specific surface area results in a significant enhancement of the fiber-substrate interfacial contact area, which in turn produces a stronger interfacial shear stress transfer effect [53]. This enhanced interfacial interaction ultimately gives PE-EGC composites excellent impact energy absorption properties.

4.5. Comparison of impact resistance

In this study, by comparing and analyzing the performance differences between PVA and PE fibers under low-speed impact, combined with the benchmark data of fly ash ECC in the literature [24], it was found that (fiber doping are 2 % volume fraction), despite the differences in raw material parameters, water-cement ratio, and impact height of the different specimens, the differences in these variables can be ultimately characterized by the three key indexes of the maximum impact force, the maximum impact displacement, and the energy dissipation coefficient These differences can be effectively characterized by three key indicators(Fig. 12):

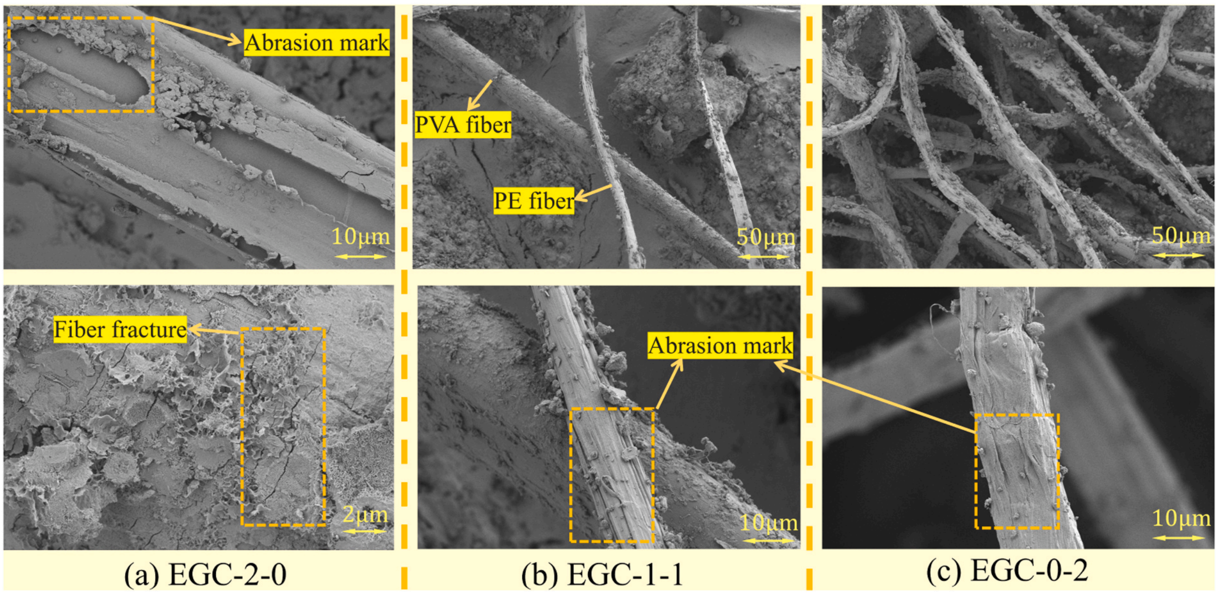

Fig. 11. Microscopic morphology of impact specimen.

maximum impact force, maximum impact displacement and energy dissipation coefficient. The experimental data show that the impact force distribution of the specimen under low velocity impact is in the range of 4500–7000 N, the impact displacement is concentrated in the range of 1–4 mm, and the energy dissipation coefficient is in the range of 65 %-99 %. It is worth noting that the impact stiffness shows a significant sensitivity to the impact height and the elastic modulus of the material but does not establish a clear linear relationship with the energy dissipation coefficient.

Comparative test data show that the average impact force of the PVA fiber specimen is increased by 16.5 % compared with that of the PE fiber specimen, but its average impact displacement and energy dissipation coefficient are reduced by 26 % and 3 %, respectively. This phenomenon is consistent with the findings of the specimen damage pattern and fiber micromorphology analysis: Compared to PE fiber specimens, the PVA fiber enhances the material stiffness through interfacial reinforcement but leads to a decrease in impact toughness [54]. Although the two types of fibers have similar energy dissipation capacity in the unbroken stage, the PVA fiber specimens are more likely to fail at high impact energy due to their brittle damage tendency. In summary, PE fiber specimens show better impact resistance at high impact energy, and their unique ductile damage mechanism not only effectively slows down the structural failure process, but also significantly improves the post-impact crack control ability through the multi-crack development mechanism [55].

5. Comprehensive performance analysis

To more accurately evaluate the comprehensive performance of each EGC ratio group, the Technique for Order of Preference by Similarity to Ideal Solution (TOPSIS) method was used to evaluate five performance indicators: tensile ductility, compressive strength, impact energy dissipation capacity, cost, and embodied carbon. The specific process was calculated using the following formula [51, 56]:

A total of five mix designs need to be evaluated, and each mix design has five evaluation indicators, which constitute the normalized matrix X:

$$X = \begin{bmatrix} x_{11} & \cdots & x_{15} \\ \vdots & \ddots & \vdots \\ x_{51} & \cdots & x_{55} \end{bmatrix} \tag{6}$$

Transform the normalized matrix X into the normalized matrix Z:

$$Z = \begin{bmatrix} z_{11} & \cdots & z_{15} \\ \vdots & \ddots & \vdots \\ z_{51} & \cdots & z_{55} \end{bmatrix} \tag{7}$$

$$z_{ij} = \frac{x_{ij}}{\sqrt{\sum_{i=1}^{n} x_{ij}^2}} \tag{8}$$

Calculation of positive $Z^+$and negative Z^-ideal solutions:

$$Z^+ = (Z_1^+, Z_2^+, \cdots, Z_5^+) = (\max\{z_{11}, z_{21}, \cdots, z_{51}\}, \cdots, \max\{z_{15}, z_{25}, \cdots, z_{55}\}) \tag{9}$$

$$Z^- = (Z_1^-, Z_2^-, \cdots, Z_5^-) = (\min\{z_{11}, z_{21}, \cdots, z_{51}\}, \cdots, \min\{z_{15}, z_{25}, \cdots, z_{55}\}) \tag{10}$$

The distance to the positive ideal solution D_i^+ and the distance to the negative ideal solution D_i^- are calculated using the following formula, where ω_j is the weight of each performance indicator:

$$D_i^+ = \sqrt{\sum_{j=1}^{n} \omega_j (Z_j^+ - z_{ij})^2} \tag{11}$$

$$D_i^- = \sqrt{\sum_{j=1}^{n} \omega_j (Z_j^- - z_{ij})^2} \tag{12}$$

The higher the value of Relative proximity S_i, the better the scheme under this weight, which is calculated using the following formula:

$$S_i = \frac{D_i^-}{D_i^- + D_i^+} \tag{13}$$

The data used for calculations are shown in Table 5, where the impact energy dissipation capacity was calculated as the energy dissipation coefficient at 12 J. Raw material prices are based on average market prices in Nanjing in 2025. The statistics of experimental results are shown in Table 6.

The weights used for the calculations are shown in Table 7, with Weight-1 equally distributing the weights of each performance metric to reflect the comprehensive performance assessment under no-preference conditions.

Weight-2 significantly increases the tensile performance and cost weights to highlight the key differences for the fiber-reinforced EGC material properties. Similarly, Weight-3 focuses on mechanical performance indicators, while Weight-4 focuses on economic and

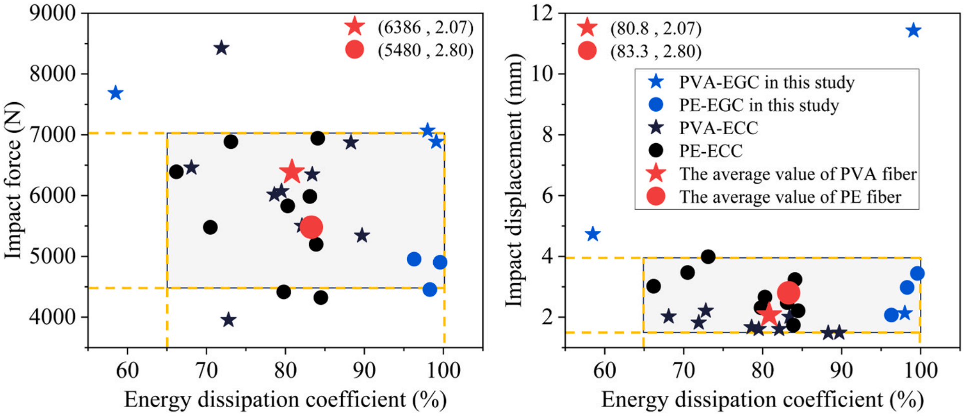

Fig. 12. Comparison of impact resistance.

Table 5
Statistics of experimental results.

Raw materials	Material cost (CNY/t)	Embodied carbon (kg CO_2/t)
Fly ash [51]	0	4
GGBS [51]	200	42
CCS [57]	100	9.22
ASM [58]	3600	1320
River sand [59]	80	2.51
HRWR [49]	4000	1880
PVA fiber [17]	40000	3400
PE fiber [17]	100000	4080

Table 6
Statistics of experimental results.

	Tensile ductility (%)	Compressive strength (MPa)	Impact energy dissipation capacity (%)	Costs (CNY/t)	Embodied carbon (kg CO_2/t)
EGC−2–0	3.30	38.9	99.1	765.3	121.4
EGC−1.5–0.5	4.11	37.3	98.5	885.6	120.6
EGC−1–1	5.81	33.7	98.1	1005.5	119.7
EGC−0.5–1.5	7.86	35.8	97.8	1125.3	118.9
EGC−0–2	7.78	34.1	98.3	1245.7	118.0

environmental evaluation.

Fig. 13 shows the standard normalized performance indicators of EGC materials with different fiber ratios. The experimental results indicate that EGC-0.5–1.5 exhibits the best tensile properties, which improve with increasing PE fiber content and reach a plateau at 1.5 % content, at which point the tensile properties, compressive strength, and impact energy dissipation stabilize. It is worth noting that due to the high unit price of polyethylene fibers, material costs increase significantly with increasing PE content. In contrast, formulations with higher PVA fiber content exhibit superior compressive strength and energy dissipation performance.

Fig. 14 calculates the comprehensive performance scores (relative proximity) of each formulation using the TOPSIS method. Analysis revealed that EGC-0.5–1.5 maintains the best overall performance under different weighting conditions, with a score 10.6 % higher than the pure PE ratio (EGC-0–2). EGC-1–1 exhibits good stability, while high PVA ratios (EGC-1.5–0.5 and EGC-2–0) show minimal performance differences. Weighting analysis shows that the scoring results for average distribution (weight 1) and key

Table 7
Weight distribution table.

Number	Tensile ductility	compressive strength	Impact energy dissipation capacity	Costs	Embodied carbon
Weight−1	0.2	0.2	0.2	0.2	0.2
Weight−2	0.3	0.1	0.2	0.3	0.1
Weight−3	0.3	0.3	0.2	0.1	0.1
Weight−4	0.15	0.15	0.1	0.3	0.3

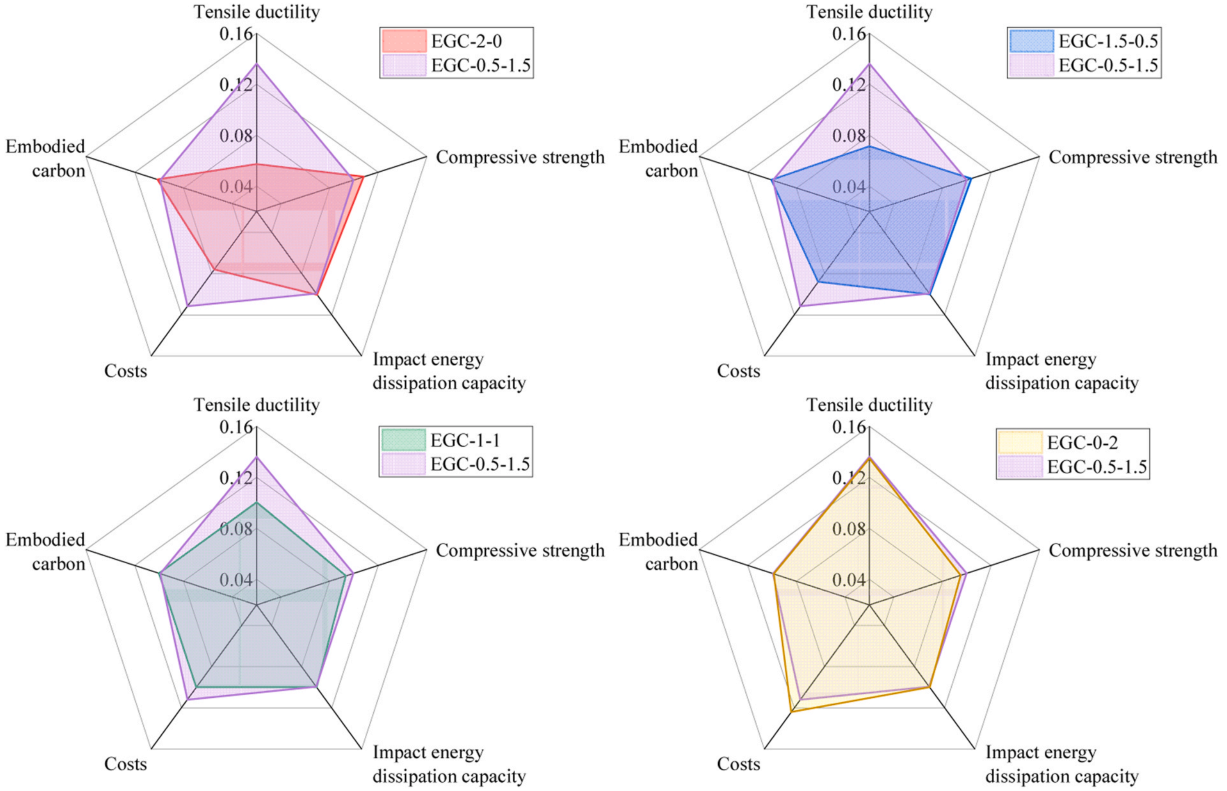

Fig. 13. Standardized values.

indicator differentiation (weight 2) are similar, indicating good consistency in the evaluation system. Specifically, under weight 3, which emphasizes mechanical performance, the scores for PE-containing ratios increased by 23 %-28 %, while those for high PVA ratios decreased by 34 %-40 %; under cost weight 4, the differences between ratios were significantly reduced.

Based on the comprehensive research results, in engineering applications with low tensile ductility requirements and cost control needs (such as commercial buildings, industrial plants, etc.), PVA fiber-reinforced EGC demonstrates significant advantages, with superior compressive strength, crack control capability, and cost-effectiveness compared to PE-reinforced ratios. However, for structures requiring high toughness or impact resistance (such as seismic components, bridge expansion joints, protective engineering, etc.), a mixture containing 1 %-1.5 % PE fibers is recommended. This formulation can enhance material ductility by 76 %-138 % while maintaining good impact energy dissipation capability, and can control crack width to within 1 mm via the fiber bridge effect.

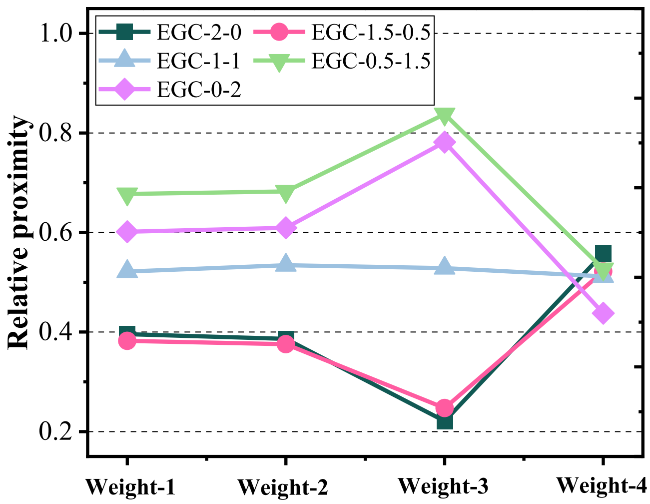

Fig. 14. Relative proximity with different weights.

However, it should be noted that this results in a 31 %-47 % increase in cost. In addition, compared to regular ECC, EGC reduces carbon emissions by 78 %, providing significant environmental benefits [4].

6. Conclusion

In this study, the mechanical properties of PVA/PE hybrid fiber-reinforced engineered geopolymer composites were systematically investigated, with mechanical response mechanism and damage evolution law under the effect of low-velocity impact, and the following conclusions were obtained based on the experimental results:

1. The evolution of the matrix-fiber interface shows stage-by-stage characteristics. At the early stage of curing, PVA fibers enhance the early strength through hydrogen bonding, while PE fibers have lower strength due to interfacial defects; at the late stage of curing, matrix densification dominates the strength development, and the difference in compressive strength between different proportions is reduced to less than 15 %.
2. PVA and PE fibers show significant complementary effects: PVA fibers form a strong interfacial bond through hydroxyl bonding and achieve multi-seam cracking under pseudo-static loading; PE fibers dominate the dynamic response through frictional slip energy dissipation by virtue of their high specific surface area and hydrophobicity; the synergy of the two fibers optimizes the balance of the tensile strength (4.48 MPa) and ductility (5.81 %).
3. The material properties showed significant strain rate effects. In pseudo-static loading (0.0001 s^{-1}), the PVA fiber system showed better crack width control than the PE system; however, under low-velocity impact loading (1–10 s^{-1}), the PE fiber system exhibited superior damage tolerance through a dense crack network.
4. Based on the standardized evaluation system, PE/PVA fiber hybrid system (EGC-0.5–1.5) has a comprehensive advantage in tensile ductility (7.86 %), tensile strength (3.85 MPa), and it has better crack control performance during the impact process, which makes it suitable for high-impact demand scenarios (piers for cross-sea bridges, offshore wind power infrastructure, etc.); The pure PVA fiber hybrid system (EGC-2–0) controls the tensile crack width at about 39 μm through the fiber bridging effect, and at the same time reduces the cost by 14–39 % compared with the PE fiber system, which is suitable for the engineering scenarios that have strict crack control requirements and need to take into account the economy (protective layer for harbor splash zone, etc.).

In addition, this study mainly conducted impact tests on samples under standard laboratory curing conditions and did not consider the effects of real marine environments (such as salt spray corrosion and dry-wet cycles) on material performance. Furthermore, the study did not cover high strain rate (10–100 s^{-1}) impact response scenarios, such as extreme load conditions caused by ship collisions and explosions. Future research should conduct in-depth exploration of the above shortcomings.

CRediT authorship contribution statement

Kai Zhou: Software. **Qian Zhang:** Formal analysis. **Haoliang Wu:** Funding acquisition. **Ke Zhuang:** Writing – review & editing, Project administration. **zhou yichen:** Writing – review & editing, Writing – original draft. **Yun Xu:** Writing – original draft, Conceptualization. **Jingming Cai:** Project administration. **Zhenqiu Hu:** Investigation. **Ziqun Wang:** Investigation. **Xiaohuan Meng:** Supervision. **Boyin Ding:** Methodology.

Declaration of Competing Interest

The authors declare that they have no known competing financial interests or personal relationships that could have appeared to influence the work reported in this paper.

Acknowledgments

This work was funded by the Natural Science Foundation of Jiangsu Province of China (BK20231430), the Fundamental Research Funds for the Central Universities (No.2242022k30030 and No.2242022k30031), the Natural Science Foundation of China (Grant No. 52408310), Guangdong Provincial Department of Science and Technology (2021ZT09G087), and Guangdong Basic and Applied Basic Research Foundation (2024A1515012528).

Data Availability

Data will be made available on request.

References

[1] H. Zhu, D. Zhang, T. Wang, H. Wu, V.C. Li, Mechanical and self-healing behavior of low carbon engineered cementitious composites reinforced with PP-fibers, Constr. Build. Mater. 259 (2020) 119805.
[2] V.C. Li, On engineered cementitious composites (ECC) a review of the material and its applications, J. Adv. Concr. Technol. 1 (3) (2003) 215–230.
[3] H. Ma, Z. Zhang, Paving an engineered cementitious composite (ECC) overlay on concrete airfield pavement for reflective cracking resistance, Constr. Build. Mater. 252 (2020) 119048.

[4] Y. Zhou, Z. Hu, X. Sui, H. Shi, Y. Lin, J. Pan, N. Ukrainczyk, J. Cai, Low-velocity impact behavior of one-part engineered geopolymer composite under extreme temperatures, Compos. Part A Applied Sci. Manuf. (2025) 108739.
[5] F. Wang, J. Ma, Y. Ding, J. Yu, K. Yu, Engineered geopolymer composite (EGC) with ultra-low fiber content of 0.2, Constr. Build. Mater. 411 (2024) 134626.
[6] L. Kan, Y. Gan, L. Lv, W. Dai, L. Dai, L. Zhang, F. Wang, Red Mud-derived Activator to Develop Greener Engineered Geopolymer Composite, Ceramics International, 2024.
[7] J.-C. Lao, R.-Y. Ma, L.-Y. Xu, Y. Li, Y.-N. Shen, J. Yao, Y.-S. Wang, T.-Y. Xie, B.-T. Huang, Fly ash-dominated high-strength engineered/strain-hardening geopolymer composites (HS-EGC/SHGC): influence of alkalinity and environmental assessment, J. Clean. Prod. 447 (2024) 141182.
[8] H. Zhong, M. Zhang, Engineered geopolymer composites: a state-of-the-art review, Cem. Concr. Compos. 135 (2023) 104850.
[9] N.P. Asrani, G. Murali, K. Parthiban, K. Surya, A. Prakash, K. Rathika, U. Chandru, A feasibility of enhancing the impact resistance of hybrid fibrous geopolymer composites: experiments and modelling, Constr. Build. Mater. 203 (2019) 56–68.
[10] Y. Lin, C. Yang, H. Shi, Y. Wang, Z. Zong, H. Qian, S. Hou, S. Li, T. Chen, J. Cai, Dynamic mechanical properties of one-part ultra-high performance geopolymer concrete, J. Build. Eng. 95 (2024) 110173.
[11] C. Thong, D. Teo, C. Ng, Application of polyvinyl alcohol (PVA) in cement-based composite materials: a review of its engineering properties and microstructure behavior, Constr. Build. Mater. 107 (2016) 172–180.
[12] S. Zhou, L. Xie, Y. Jia, C. Wang, Review of cementitious composites containing polyethylene fibers as repairing materials, Polymers 12 (11) (2020) 2624.
[13] Y. Xu, C. Wan, X. Liang, H. Yang, The reinforcement effects of PVA, PE, and steel fibers on AAS material, Case Stud. Constr. Mater. 17 (2022) e01386.
[14] S. Zhang, E. Duque-Redondo, A. Kostiuchenko, J.S. Dolado, G. Ye, Molecular dynamics and experimental study on the adhesion mechanism of polyvinyl alcohol (PVA) fiber in alkali-activated slag/fly ash, Cem. Concr. Res. 145 (2021) 106452.
[15] K. Hannawi, H. Bian, W. Prince-Agbodjan, B. Raghavan, Effect of different types of fibers on the microstructure and the mechanical behavior of ultra-high performance fiber-reinforced concretes, Composites Part B Engineering 86 (2016) 214–220.
[16] Z. Pan, C. Wu, J. Liu, W. Wang, J. Liu, Study on mechanical properties of cost-effective polyvinyl alcohol engineered cementitious composites (PVA-ECC), Constr. Build. Mater. 78 (2015) 397–404.
[17] B.-Y. Deng, L.-Z. Li, D. Tan, M.N. Uddin, Z.-W. Cai, K.-Q. Yu, Sustainable and cost-effective ultra-lightweight engineered cementitious composite: Design and material characterization, Cem. Concr. Compos. 136 (2023) 104895.
[18] T. Cooke, Biodegradability of polymers and fibers-a review of the literature, J. Polym. Eng. 9 (3) (1990) 171–212.
[19] N. Ranjbar, M. Zhang, Fiber-reinforced geopolymer composites: a review, Cem. Concr. Compos. 107 (2020) 103498.
[20] Y. Alrefaei, J.-G. Dai, Tensile behavior and microstructure of hybrid fiber ambient cured one-part engineered geopolymer composites, Constr. Build. Mater. 184 (2018) 419–431.
[21] J. Marzbanrad, M. Alijanpour, M.S. Kiasat, Design and analysis of an automotive bumper beam in low-speed frontal crashes, Thinwalled Struct. 47 (8-9) (2009) 902–911.
[22] J.-P. Mougin, P. Perrotin, M. Mommessin, J. Tonnelo, A. Agbossou, Rock fall impact on reinforced concrete slab: an experimental approach, Int. J. Impact Eng. 31 (2) (2005) 169–183.
[23] L. Sutherland, A review of impact testing on marine composite materials: part I–Marine impacts on marine composites, Compos. Struct. 188 (2018) 197–208.
[24] J. Cai, J. Pan, Y. Lin, J. Han, B. Ding, N. Ukrainczyk, Effect of temperature on the low-velocity impact behaviors of engineered cementitious composite, J. Mater. Civ. Eng. 35 (7) (2023) 04023167.
[25] A.K. Nassar, P. Kathirvel, G. Murali, A. Krishna, Development and performance evaluation of novel sustainable one-part alkali-activated fibrous concrete subjected to drop weight impact loading: an experimental study, Constr. Build. Mater. 459 (2025) 139754.
[26] C. Zhang, G. Gholipour, A.A. Mousavi, State-of-the-art review on responses of RC structures subjected to lateral impact loads, Arch. Comput. Methods Eng. 28 (4) (2021) 2477–2507.
[27] H.H. Nguyễn, P.H. Nguyễn, Q.-H. Lương, W. Meng, B.Y. Lee, Mechanical and autogenous healing properties of high-strength and ultra-ductility engineered geopolymer composites reinforced by PE-PVA hybrid fibers, Cem. Concr. Compos. 142 (2023) 105155.
[28] K.T. Soe, Y. Zhang, L. Zhang, Impact resistance of hybrid-fiber engineered cementitious composite panels, Compos. Struct. 104 (2013) 320–330.
[29] Y. Ling, X. Zhang, Y. Wu, W. Zou, C. Wang, C. Li, W. Li, Evaluation of bonding behavior between engineered geopolymer composites with hybrid PE/PVA fibers and concrete substrate, Materials 17 (15) (2024) 3778.
[30] J. Guo, J. Shi, L. Wang, C. Huang, X. Tao, C. Li, Z. Chen, Evaluation of axial compressive and tensile properties of PE/PVA hybrid fiber reinforced strain-hardening geopolymer composites, Materials 17 (17) (2024) 4356.
[31] J. Temuujin, A. Van Riessen, R. Williams, Influence of calcium compounds on the mechanical properties of fly ash geopolymer pastes, J. Hazard. Mater. 167 (1-3) (2009) 82–88.
[32] L.N. Assi, E.E. Deaver, P. Ziehl, Effect of source and particle size distribution on the mechanical and microstructural properties of fly Ash-Based geopolymer concrete, Constr. Build. Mater. 167 (2018) 372–380.
[33] M. Elzeadani, D. Bompa, A. Elghazouli, One part alkali activated materials: a state-of-the-art review, J. Build. Eng. 57 (2022) 104871.
[34] W. Sun, H. Yan, B. Zhan, Analysis of mechanism on water-reducing effect of fine ground slag, high-calcium fly ash, and low-calcium fly ash, Cem. Concr. Res. 33 (8) (2003) 1119–1125.
[35] V.C. Li, Engineered cementitious composites (ECC) material, Struct. Durab. Perform. (2008).
[36] P. Rovnaník, Effect of curing temperature on the development of hard structure of metakaolin-based geopolymer, Constr. Build. Mater. 24 (7) (2010) 1176–1183.
[37] S.Y. Oderji, B. Chen, S.T.A. Jaffar, Effects of relative humidity on the properties of fly ash-based geopolymers, Constr. Build. Mater. 153 (2017) 268–273.
[38] H. Yokota, K. Rokugo, N. Sakata, JSCE Recommendations for Design and Construction of High Performance Fiber Reinforced Cement Composite With Multiple Fine Cracks, High Performance Fiber Reinforced Cement Composites, Springer, Tokyo, Japan, 2008.
[39] A. Standard, D7136: Standard Test Method for Measuring the Damage Resistance of a Fiber-reinforced Polymer Matrix Composite to a Drop-weight Impact Event, ASTM International, West Conshohocken, 2005.
[40] M. Hou, D. Zhang, V.C. Li, Crack width control and mechanical properties of low carbon engineered cementitious composites (ECC), Constr. Build. Mater. 348 (2022) 128692.
[41] A.B. Rezaie, M. Liebscher, M. Ranjbarian, F. Simon, C. Zimmerer, A. Drechsler, R. Frenzel, A. Synytska, V. Mechtcherine, Enhancing the interfacial bonding between PE fibers and cementitious matrices through polydopamine surface modification, Compos. Part B Eng. 217 (2021) 108817.
[42] M. Keskinateş, B. Felekoğlu, E. Gödek, A comprehensive experimental study on the role of matrix structure on the multiple cracking behavior of PVA-ECC, Theor. Appl. Fract. Mech. 121 (2022) 103503.
[43] L. Li, Z. Cai, K. Yu, Y. Zhang, Y. Ding, Performance-based design of all-grade strain hardening cementitious composites with compressive strengths from 40 MPa to 120 MPa, Cem. Concr. Compos. 97 (2019) 202–217.
[44] S. He, Z. Li, E.-H. Yang, Quantitative characterization of anisotropic properties of the interfacial transition zone (ITZ) between microfiber and cement paste, Cem. Concr. Res. 122 (2019) 136–146.
[45] K. Yu, Y. Ding, J. Liu, Y. Bai, Energy dissipation characteristics of all-grade polyethylene fiber-reinforced engineered cementitious composites (PE-ECC), Cem. Concr. Compos. 106 (2020) 103459.
[46] H. Zhong, M. Zhang, Effect of recycled polymer fibre on dynamic compressive behaviour of engineered geopolymer composites, Ceram. Int. 48 (16) (2022) 23713–23730.
[47] E.-H. Yang, S. Wang, Y. Yang, V.C. Li, Fiber-bridging constitutive law of engineered cementitious composites, J. Adv. Concr. Technol. 6 (1) (2008) 181–193.
[48] S. Dong, Y. Tan, Q. Lu, G. Liu, C. Gao, Y. Cao, Physicochemical properties of PVA and PE fibers and their impact on the mechanical properties of cement-based composite materials. International Conference on Geosynthetics and Environmental Engineering, Springer, 2024, pp. 315–328.

[49] Z. Zhang, F. Qin, H. Ma, L. Xu, Tailoring an impact resistant engineered cementitious composite (ECC) by incorporation of crumb rubber, Constr. Build. Mater. 262 (2020) 120116.
[50] J. Cai, J. Pan, J. Han, Y. Lin, Z. Sheng, Low-energy impact behavior of ambient cured engineered geopolymer composites, Ceram. Int. 48 (7) (2022) 9378–9389.
[51] H. Ye, B. Zhu, P. Ping, Y. Lin, J. Cai, J. Pan, Mechanical performance, impact behavior and environmental assessment of coal furnace slag based low-carbon ultra-high performance engineered cementitious composites (UHP-ECC), J. Clean. Prod. 450 (2024) 141921.
[52] H. Li, W.-J. Long, K.H. Khayat, Efficient recycling of waste rubber in a sustainable fiber-reinforced mortar and its damping and energy dissipation capacity, Cem. Concr. Compos. 138 (2023) 104963.
[53] C.-S. Tang, B. Shi, L.-Z. Zhao, Interfacial shear strength of fiber reinforced soil, Geotext. Geomembr. 28 (1) (2010) 54–62.
[54] N. Elmesalami, K. Celik, A critical review of engineered geopolymer composite: a low-carbon ultra-high-performance concrete, Constr. Build. Mater. 346 (2022) 128491.
[55] Y. Ling, X. Zhang, W. Zou, C. Feng, H. Lai, J. Yang, B. Xie, Axial impact resistance of high-strength engineering geopolymer composites: effect of polyethylene fiber content and strain rate, Buildings 14 (5) (2024) 1438.
[56] M. Behzadian, S.K. Otaghsara, M. Yazdani, J. Ignatius, A state-of the-art survey of TOPSIS applications, Expert Syst. Appl. 39 (17) (2012) 13051–13069.
[57] X. Li, W. Ma, S. Li, S. Hou, Y. Chen, X. Wen, J. Dan, J. Huang, Y. Lv, Study on the properties and carbon footprint of low heat cement clinker prepared by recycled concrete powder and calcium carbide slag, Constr. Build. Mater. 441 (2024) 137542.
[58] K.-H. Yang, J.-K. Song, K.-I. Song, Assessment of CO2 reduction of alkali-activated concrete, J. Clean. Prod. 39 (2013) 265–272.
[59] W. Chen, S. Yang, X. Zhang, N.D. Jordan, J. Huang, Embodied energy and carbon emissions of building materials in China, Build. Environ. 207 (2022) 108434.